Morphological Phase Diagram for a Ternary System of Block Copolymer PS_{310}-*b*-PAA_{52}/Dioxane/H_2O

Hongwei Shen and Adi Eisenberg*

Department of Chemistry, McGill University, 801 Sherbrooke Street West, Montreal, Quebec, Canada H3A 2K6

Received: April 26, 1999; In Final Form: August 29, 1999

The partial ternary phase diagram was investigated for the polystyrene$_{310}$-*block*-poly(acrylic acid)$_{52}$ copolymer in dioxane/water mixtures in regions in which self-assembled nanoaggregates of various morphologies are seen. Both fractionated and unfractionated copolymers were used; the unfractionated copolymer contains homopolystyrene. The study was carried out over the range of water contents from 0 to 45 wt % and copolymer concentrations from 0.1 to 10 wt %. Freeze-drying transmission electron microscopy (TEM), turbidity measurements, as well as static and dynamic light scattering were employed. Because of the proximity of the melting points and boiling points of water and dioxane, quenching and subsequent freeze-drying of solution samples can be employed to preserve aggregate morphologies. The morphologies can then be observed using TEM. The reversibility of various morphological transitions was examined by means of TEM and turbidity measurements. With increasing water content, the sequence of copolymer structures in solution follows the order of single chains, spheres, sphere and rod mixtures, rods, rod and vesicle mixtures, and finally pure vesicles. The morphologies observed here are under thermodynamic control. Not only the water content but also the polymer concentration affects the morphologies and the sizes of the aggregates. For the unfractionated polymer, the single-chain/sphere boundary shifts to lower water contents relative to that of the fractionated copolymer, while the other morphological boundaries move to higher water contents. On the basis of the progressive changes of the aggregate morphologies with the addition of water, possible pathways of the morphological transitions are suggested and discussed briefly. Also, approximate thermodynamic functions are estimated for the morphological transitions on the basis of the morphological boundaries. The combination of freeze-drying TEM techniques with turbidity measurements is very useful in exploring the morphological behavior of block copolymers in solution.

1. Introduction

Micellization of block copolymers in selective solvents has been studied extensively, and a number of reviews have appeared.[1] Amphiphilic copolymers can self-assemble in aqueous media to give regular micelles with a hydrophobic core and a hydrophilic corona, or they can aggregate in organic solvents to give reverse micelles with the hydrophilic block in the core. Because most of the previous studies dealt with starlike micelles (both regular and reverse) formed from copolymers with relatively long corona-forming blocks, the micelles are mainly spherical.[1] Some nonspherical morphologies were suggested on the basis of light scattering and small-angle X-ray scattering measurements.[2] Nonspherical aggregates were rarely observed using TEM.[3] Crew-cut aggregates with a relatively large core and short corona have been receiving attention only recently.[4−16] By contrast to starlike micelles, various morphologies were observed from these aggregates in both aqueous[6−13] and organic media.[14−16] The morphologies include spheres, rods, bicontinuous rods, lamellae, vesicles, large compound micelles (LCMs), large compound vesicles (LCVs), hexagonally packed hollow hoops (HHHs), and many others.[6−16]

The various morphologies of nanoaggregates formed form block copolymers, especially from polystyrene-*b*-poly(acrylic acid) (PS-*b*-PAA), have been intensively investigated in our group.[6−12] It has been found that the morphologies are influenced by many variables, e.g., the composition of the block copolymers, the copolymer concentration, the type of the common solvent, the type and concentration of added ions, and others. A typical preparation of the aggregates involves the dissolution of copolymers in an organic solvent (e.g., DMF), the dropwise addition of deionized water, and finally the dialysis of the mixtures against distilled water.[6] Alternately, direct dissolution of copolymers in a mixed solvent followed by quenching can also result in the formation of both spherical and nonspherical aggregates.[11] However, due to the slow chain dynamics at relatively high water contents, e.g., above ca. 7 wt % (in DMF), the aggregation behavior cannot be explored at those high water contents.[9] At high temperature and high pressure, various morphologies can also be formed by the dissolution of copolymers into a single solvent, e.g., alcohol.[12]

Although the influence of many variables on the formation of various aggregates from block copolymers has been investigated, fundamental questions regarding the equilibrium nature of morphologies other than solid spheres have not yet been answered. The determination of a morphological phase diagram

* To whom correspondence should be addressed. E-mail: eisenber@chemistry.mcgill.ca.

10.1021/jp991365c CCC: $18.00
Published on Web 10/14/1999

can certainly answer the above question. In addition, such a study can also show quantitatively how the water content, polymer concentration, and homopolystyrene content affect the aggregate morphologies. Therefore, it is of fundamental importance to explore the morphological phase diagram of the strongly amphiphilic block copolymers in very dilute solution. However, so far, no such attempts have been made.

Phase diagrams of block copolymers in bulk have been extensively investigated for many years.[17−22] These phase diagrams usually show two disordered phases and several ordered phases. In the ordered region, seven equilibrium phases and four nonequilibrium or metastable phases have been identified.[22] Five of the classical equilibrium phases (or morphologies), including two cubic phases (Sphere), two hexagonally packed cylinder phases (HEX), and one lamellar phase (LAM), were identified using TEM.[17] The other two equilibrium phases are the bicontinuous cubic phases (Gyroid), which were identified recently with the help of small-angle X-ray scattering.[19] All these equilibrium phases are predictable from theoretical studies.[17,18] The four nonequilibrium phases include two unstable OBDD bicontinuous phases and two metastable perforated lamellar phases.[22] It should be noted that, generally, not all the phases can appear in a single copolymer series. The melt morphologies can be preserved by annealing followed by quenching and can then be studied by TEM or other techniques.[17] Due to the kinetic difficulties encountered in the sample preparation, it is clear that careful handling of the samples is crucial to avoid misidentification.[22]

Solutions of small molecule surfactants, which bear some relation to the present work, have also been studied extensively for many decades.[23−27] Various phases are present in small molecule surfactant systems. In addition to the ordered phases, I_1 and I_2 (Spheres), H_1 and H_2 (HEX), V_1 and V_2 (Gyroid), and L_α (LAM), which also appear in the bulk copolymer systems, other morphologies, including spheres, rods, irregular bicontinuous, and bilayers, occur in the disordered phase.[26,27] No metastable phases have been observed among the ordered phases because the kinetics are rapid in the small molecule surfactant systems.[24,25]

One disordered bilayer phase, the vesicle, had been commonly regarded as a nonequilibrium structure[25] until the formation of vesicles from a mixture of surfactants reopened the question about a decade ago.[28−36] Theoretical studies show that if a mixture of surfactants or a mixture of a surfactant and other polar molecules can provide different curvatures at two sides of the bilayers, thermodynamically stable vesicles can, indeed, exist.[32−35] In some experimental studies, vesicles prepared from various mixtures are claimed to be an equilibrium morphology.[28−30] However, other workers who challenge this concept believe that the vesicle is a form of an irreversible colloid structure.[36]

The solution behavior of poly(ethylene oxide) (PEO) based copolymers has been studied for some years.[37−43] Recently, it was found that nine equilibrium phases are present in a PPO/PEO−water−oil system.[43] These equilibrium phases include two disordered phases, L_1 and L_2 (regular and reverse micelles), and seven ordered phases which are also found in solutions of small molecule surfactants. In the PEO based copolymer systems, the time scale used to reach equilibrium varies from days to weeks.[38,41] It is believed that the copolymers in bulk and in concentrated or semidilute solutions share the same principles that govern their phase behavior.[42] Theoretically, vesicles could be achieved in concentrated or semidilute copolymer solutions.[44] However, experimentally, no vesicles have been seen in these systems.[37−45]

For the present study, the PS-*b*-PAA diblock family was selected since many studies have been performed on the morphological aspects of the system.[6−12] Dioxane was chosen to be the common solvent because the melting point and boiling point are close to those of water, the precipitant for the PS block.[46] Since the morphological transitions of interest occur at relatively low water contents and low copolymer concentrations, the present study was performed in the water content range of 0 to 45 wt % at polymer concentrations of 0.1 to 10 wt %. Although the chain exchange rate constants in the micellization of copolymers are generally very slow (i.e., 10^{-6} to 10^{-3} s^{-1} for copolymer micelles versus 10^6 to 10^8 s^{-1} for conventional surfactant micelles),[1,47] the rate constant increases significantly with decreasing precipitant (for the micellar core) content.[48] Since the present study was performed at relatively low water contents, the chain mobility should be fairly high. However, the solution can be rapidly frozen because of the high freezing points of dioxane and water. The solid solvent mixture can then be sublimed, and the aggregate morphology can be visualized using TEM. Therefore, equilibrium morphologies can be investigated. Furthermore, the reversibility of various morphological transitions is carefully examined using both TEM and turbidity measurements. The effects of water content, polymer concentration, and fractionation are explored in detail. The pathways of various morphological transitions upon addition of water are also briefly discussed. Finally, thermodynamic parameters for the various morphological transitions are estimated on the basis of the phase diagram.

2. Experimental Section

2.1. Block Copolymers. The polystyrene-*b*-poly(*tert*-butyl acrylate) diblock copolymers were synthesized by sequential anionic polymerization of styrene followed by *tert*-butyl acrylate (*t*-BuA) using *sec*-butyllithium as the initiator.[49] The polymerization was carried out in tetrahydrofuran (THF) at −78 °C under nitrogen. After the polystyrene block was formed, an aliquot of the reaction mixture was withdrawn for characterization. A series of diblock copolymers with the same polystyrene block length were obtained by withdrawing aliquots of the mixtures after each *t*-BuA monomer addition. The degree of polymerization of the PS blocks and the polydispersities of the homopolymers and diblocks were determined by gel permeation chromatography (GPC). FT-IR was used to determine the degree of polymerization of the poly(*t*-BuA) blocks relative to that of the PS block using a previously established calibration curve.[49] The poly(*t*-BuA) blocks in the copolymers were hydrolyzed to their acid form in toluene using *p*-toluenesulfonic acid as the catalyst. A detailed description of the procedures can be found elsewhere.[49]

In anionic polymerization, the copolymer often contains some homopolymer due to the chain termination upon the addition of the second monomer. Thus, a fractionation process is needed to purify PS-*b*-PAA copolymers; a detailed procedure was described in a previous publication.[50] To fractionate the mixture, the acrylic acid blocks were first converted to sodium acrylate in THF by addition of sodium hydroxide, which results in the immediate formation of the reverse micelles with a poly(sodium acrylate) core. Upon addition of water, the reverse micelles precipitated first because of the high molecular weight; the copolymers were then separated by removing the upper homopolystyrene solution. The above process was repeated several times until no homopolystyrene was detected in the reverse micelle phase by GPC.[50] The sodium acrylate blocks were then converted back to the acrylic acid form. The copolymers PS_{310}-

b-PAA_{52} and PS_{310}-*b*-PAA_{75} were used in the present study; the subscript labels indicate the number of repeat units in the blocks. Both copolymers have a polydispersity index of 1.05.

2.2. Light Scattering Measurements. The light scattering experiments were performed on a Brookhaven light scattering instrument with a BI9000 AT digital correlator. The instrument is equipped with an Uniphase μBlue laser with an output power of 125 mW, which supplies vertically polarized light with a wavelength of 532 nm. The data were collected by monitoring the scattered light intensity at a 90° scattering angle at 25 °C. The stock solutions (1−10 wt %) were prepared by dissolving the diblocks in dioxane, which is a common solvent for both blocks, and were stored overnight in covered glass tubes sealed with Teflon tape. These stock solutions were filtered directly into the scintillation vials of 1.5 cm diameter through filters of 0.45 μm pore size, and diluted with filtered dioxane solvent to the desired copolymer concentrations. Deionized water (filtered through filters of 0.22 μm pore size) was added dropwise at a rate of 0.2 wt % per minute to form the aggregates. Static light scattering (SLS) measurements were performed after each sample was allowed to sit at a given water content for 20 min. Each of the water increment steps was ca. 1 wt %. Dynamic light scattering (DLS) measurements were used as a monitor for the phase diagram study. Thus, data were taken at water intervals that are the same as those in the phase diagram study (see section 2.4). The filters were always rinsed first with solvent and/or the stock solution before the filtration of solvent and stock solutions, as described in a previous paper.[50]

2.3. Turbidity Measurements. Turbidity measurements were performed on an 8452A diode array UV−visible spectrophotometer (Hewlett-Packard) using HP 89531A MS-DOS UV/vis Operation Software. The measurements were carried out at a wavelength of 650 nm where the absorption is lowest for both polymer and aggregate solutions. Dioxane was used as the reference for all the measurements. The preparation of the solution samples was the same as that for SLS measurements (see section 2.2).

2.4. Sample Preparation for the Phase Diagram Study. The sample preparation was similar to that for SLS measurements (see section 2.2). However, at each water increment (ca. 2 wt % after aggregation), samples were stored for 3 or 4 days when the water content was below 20 wt % and for 1 week for samples above 20 wt % water. Although optical observations and turbidity measurements suggest that the time scale needed to reach equilibrium is in the range of several minutes to an hour, depending on the water content (see section 3.1.1), extra time was taken to make sure that equilibrium had been reached before the samples were prepared for TEM observation. In some cases, the samples were stored in solution for periods exceeding 2 years to examine the stability of various aggregates.

2.5. Freeze-Drying Transmission Electron Microscopy. Transmission electron microscopy (TEM) was performed on a Phillips EM400 microscope operating at an acceleration voltage of 80 kV. EM copper grids were first coated with a thin film of Formvar (J.B. EM Services Inc.) and a film of carbon. Then, to avoid the possible artifacts from exposing the Formvar film to the solvent (dioxane), the coated EM grids were kept in acetone with gentle stirring for a week to remove the Formvar film. After eliminating the Formvar film, the EM grids, coated only with carbon, were used for the present study. For the observation of the aggregate morphologies, ca. 0.01 mL of each sample was withdrawn from the solutions used in the phase diagram study (section 2.4) and deposited onto the carbon coated EM copper grids. A thin layer of the liquid sample on the copper grids was immediately frozen by putting it on a metal block which was kept in thermal equilibrium with liquid nitrogen and then freeze-dried under vacuum for 2 days. Finally, the samples were shadowed with a palladium/platinum alloy at an angle of ca. 35°. The sizes of aggregates were measured directly from the prints of the microscope negatives after calibration using a standard PS latex.[6] In the course of TEM observation, it was noted that the morphologies are completely stable in a weak electron beam, but exposure of the sample to a strong electron beam results in the extensive deformation of the aggregates. Therefore, only weak electron beams were used.

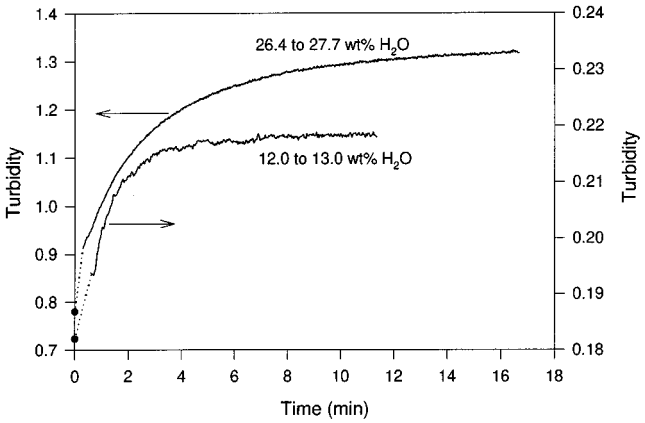

Figure 1. Plots of the turbidity against time for a 1.00 wt % fractionated PS_{310}-*b*-PAA_{52}. The dotted lines are the extension of the curves to zero time.

3. Results and Discussion

The Results and Discussion section is divided into five parts. The first presents the evidence that the morphologies observed here represent equilibria. The evidence involves both thermodynamic and kinetic arguments. The second part is devoted to the determination of the phase diagrams of the fractionated and unfractionated copolymer PS_{310}-*b*-PAA_{52} in dioxane/water mixtures. The effects of water content, polymer concentration, and fractionation are described in detail. In the third part, the pathways of the morphological transitions accompanying water addition are discussed. In part four, thermodynamic functions are estimated on the basis of the phase diagram. In the final part, a comparison is given of the present phase diagram with those of block copolymers in bulk, of small molecule surfactants in solution, and of PEO based copolymers in concentrated solution.

3.1. Equilibrium Morphologies. *3.1.1. Kinetic Considerations.* The study of thermodynamic aspects of self-assembly of high molecular weight copolymers frequently encounters difficulties involving kinetics. Therefore, it is essential to explore the kinetics of the self-assembly process before an observed morphology can be identified as an equilibrium phase. A previous study of the dynamics of high molecular weight chains in dioxane/water mixtures revealed that the exchange rate constant depends strongly on the composition of the solvent mixture.[48] Thus, one can anticipate that in the present case the chain mobility should also be a function of the solvent composition.

Figure 1 shows plots of the turbidity as a function of time for the 1.00 wt % fractionated copolymer PS_{310}-*b*-PAA_{52} for ca. 1 wt % water jumps at two different water contents. The dotted lines connect the starting points ($t = 0$) with the earliest attainable experimental points. The lower curve, obtained for a water content jump from 12.0 to 13.0 wt %, reaches a plateau

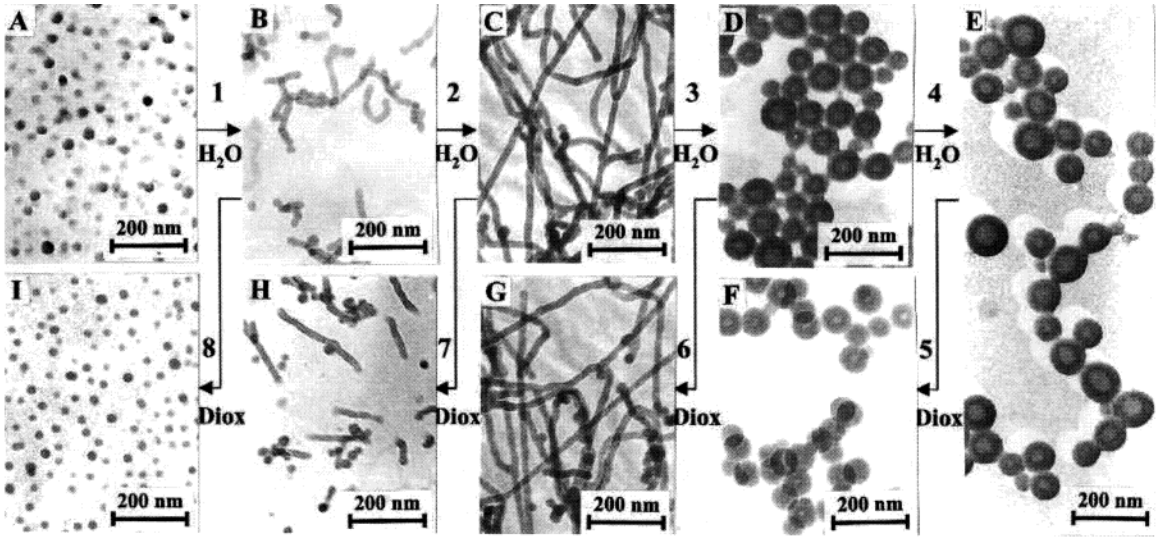

Figure 2. Reversibility of various morphological transitions for 1.00 wt % of fractionated copolymer PS_{310}-*b*-PAA_{52} solution. The arrows indicate the directions of morphological changes on addition of water (steps 1−4) or dioxane (steps 5−8): (A) spheres at 9.1 wt % water; (B) short rods upon addition of water to 11.5 wt %; (C) long rods at 14.0 wt % water; (D) vesicles at 28.0 wt % water; (E) bigger vesicles at 40 wt % water; (F) back to smaller vesicles at 29 wt % water by adding dioxane to sample E; (G) back to long rods at 14 wt % water upon addition of dioxane to sample F; (H) back to short rods at 11.8 wt % of water upon addition of dioxane to sample G; (I) back to spheres at 9.5 wt % water by adding dioxane to sample H.

in ca. 5 min, which indicates that most of the morphological changes triggered by water addition are complete within that time frame. The upper curve, obtained for a water content jump from 26.4 to 27.7 wt %, levels out in ca. 15 min. Clearly, the chain mobility decreases with increasing water content, but is not very slow in either case. The lower curve is a reflection of the process of sphere-to-rod transition, while the upper one corresponds to the process of vesicle formation from rods (see discussion of phase diagrams in sections 3.2.1 and 3.2.2). As seen from Figure 1, rod formation from spheres is clearly faster than vesicle formation from rods. Thus, the chain dynamics or kinetics of morphological transitions are faster at low water contents, which is in agreement with the previous results.[48] Both plateau regions were monitored for a period of a week. No changes in the turbidity were observed after 15 min for the lower curve or after 40 min for the upper curve. Therefore, both morphological transitions are complete over those time scales. A detailed kinetic analysis is presented in the following paper of the same issue.[51] In addition, the aggregate morphologies have been observed using TEM for an extended time period (see section 3.1.2).

The kinetics of morphological changes are determined not only by the water content but also by the magnitude of the water content jump. It has been shown in preliminary experiments that a large water content jump, which one might want to use to induce rapid morphological reorganization, can result instead in freezing or quenching of nonequilibrium morphologies. Also, previous experiments showed that the dissolution of a copolymer directly into a solvent mixture at relatively high water contents can result in the formation of nonequilibrium aggregates due to slow chain dynamics.[11] Therefore, the aggregates in the phase diagram study should be prepared by slow water addition. After each water addition, sufficient time should be allowed to pass for the system to regain equilibrium, a phenomenon similar to the annealing process in bulk studies. It was suggested that the indirect way as employed here is a practical method to prepare equilibrium aggregates of copolymers in solution.[52]

3.1.2. Stability of Various Morphologies. The aggregate morphologies should not change with time if they are equilibrium phases. As one test of whether they are true equilibrium morphologies, we examined the aggregates as a function of time over long time periods. Up to now, solutions of spherical, rodlike, and vesicular aggregates have been stored under preparation conditions for over 14, 14, and 24 months, respectively. At intervals of 1 to 2 months, a drop of each of these samples was withdrawn and freeze-dried for TEM observation. So far, all the aggregate morphologies in the solvent mixtures have remained unchanged. However, the stability of the morphologies alone is not sufficient to prove their equilibrium nature. To prove the existence of true equilibria, it is necessary to demonstrate that the same morphologies can be obtained reversibly both with increasing and decreasing water contents.

3.1.3. Reversibility of Various Morphological Transitions. Previous experiments using SLS showed that the spheres are thermodynamically controlled morphologies.[50] Naturally, it is also of interest to inquire whether the shapes and the dimensions of the short rods, long rods, and vesicles are also under thermodynamic control. To explore this aspect, we tested the reversibility of morphological transitions by inducing a shape change upon the addition of water, and subsequently monitoring its return to the starting morphology following the addition of dioxane. Changes in the aggregate dimensions were also monitored. Figure 2 shows TEM pictures obtained in the above experiments utilizing a 1.00 wt % fractionated copolymer PS_{310}-*b*-PAA_{52} solution. Figure 2A shows spheres present at 9.1 wt % water. An increase in the water content to 11.5 wt % (step 1) results in the formation of short rods shown in Figure 2B. The short rod solution was then divided into two parts. Upon addition of dioxane to one of the short rod solutions (step 8), which reduced the water content to 9.5 wt % water, spherical aggregates were reformed, as shown in Figure 2I. The continued addition of water to the other short rod solution (step 2) resulted in the formation of long rods at a water content of 14.0 wt %, as shown in Figure 2C. This solution was again split to two parts. The addition of dioxane to one part (step 7) changed the long rods back to short rods at 11.8 wt % water, as seen in Figure 2H. To the other part, water was added to 28 wt % (step

TABLE 1: Effect of the Water Content on the Vesicle Size

	photograph					
	Figure 2D	Figure 2E	Figure 2F			
polym/H_2O (wt %)	0.72/28	0.60/40	0.44/29	2.16/28	1.80/40	1.26/28
mean diameter (nm)	84.3	90.2	80.7	93.3	96.7	87.6
std. dev. (nm)	13.7	14.8	13.8	17.5	18.9	16.6
95% conf. (nm)	1.9	2.1	1.9	2.4	2.7	2.3
99% conf. (nm)	2.5	2.7	2.5	3.2	3.4	3.0
mean wall thickness (nm)	25.7	27.0	26.5	26.2	27.2	26.6
std. dev. (nm)	2.5	3.0	2.7	2.7	3.2	2.8
95% conf. (nm)	0.4	0.4	0.4	0.4	0.4	0.5
99% conf. (nm)	0.5	0.6	0.6	0.5	0.6	0.6
std. dev./mean dia.	0.16	0.16	0.17	0.19	0.20	0.19

3), where pure vesicles formed, as shown in Figure 2D. The average outside diameter of the vesicles is 84.3 nm with a wall thickness of 25.7 nm. The results of a statistical population study for these vesicles, based on 200 points, are given in Table 1. The vesicle solution was again divided into two parts. Dioxane was added to one part until the water content decreased to 14 wt % (step 6). The vesicles changed back to long rods, as shown in Figure 2G. Continued addition of water to the other part to 40 wt % water (step 4) did not change the morphology, but the size of vesicles increased to 90.2 nm with a wall thickness of 27.0 nm. The picture is shown in Figure 2E and the statistical data are also listed in Table 1. The addition of dioxane to the relatively large vesicle solution to achieve a water content of 29 wt % (step 5) results in the formation of smaller vesicles with a diameter of 80.7 nm and a wall thickness of 26.5 nm. The picture and detailed data are presented in Figure 2F and Table 1, respectively.

As seen from the experiments summarized in Figure 2, the sequence of morphologies resulting from the addition of water is spheres, short rods, long rods, small vesicles, and larger vesicles. Subsequent addition of dioxane, which decreases the water content, reverses the sequence from the relatively large vesicles to smaller vesicles, to long rods, to short rods, and finally to spheres. Reversibility has thus been demonstrated in every step of the morphological transitions. It should be noted here that the polymer concentration decreases continuously upon the addition of water followed by the addition of dioxane. In Table 1, the actual polymer concentrations are reported instead of the initial polymer concentration, i.e., 1.00 wt % for the first group or 3.00 wt % for the second. Obviously, the polymer concentration decreases significantly with each dilution. To avoid excessive dilution of the polymer solution, the reverse process for any morphology was examined by the addition of dioxane to a solution having that morphology at the highest polymer concentration. Thus, in step 6, the change of vesicles to long rods, we used solution 2D (where the polymer concentration is 0.72 wt %) instead of that shown in Figure 2F (where the polymer concentration is 0.60 wt %). Similarly, for the conversion of short rods back to spheres, we started from solution 2B (polymer concentration = 0.88 wt %) instead of solution 2H (polymer concentration = 0.73 wt %). If we had started the reverse process with the solution 2F and added dioxane to reduce the water content to 9.5 wt %, the polymer concentration would have been 0.13 wt %, which is far from the starting polymer concentration of 1.00 wt %.

Figure 3 shows the position of the starting point and end point for steps 1 through 8, giving the locations of points A through I, on a diagram which will be discussed in section 3.2.1. S, R, and V represent regions of stability of spheres, rods, and vesicles, respectively. Letter combinations (e.g., S + R) indicate the presence of mixtures of morphologies. These mixtures are also thermodynamically stable because they can be recreated

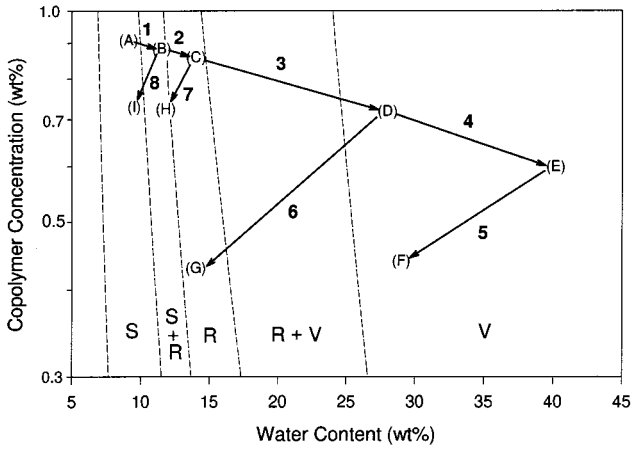

Figure 3. Locations of the reversible morphological transitions shown in Figure 2 on a simplified phase diagram (similar to that shown in Figure 6A). The arrows and numbers are the same as those in Figure 2. Letters, S, R, and V, represent spheres, rods, and vesicles, respectively.

from high water or high dioxane directions starting from the pure morphologies.

Several other starting points and end points were also utilized in the study of the reversibility to test whether more morphological jumps can be made. For example, starting from a pure vesicle solution at 34 wt % water and 0.66 wt % polymer, dioxane was added progressively to decrease the water content to 10 wt % water, which converted the vesicles back to long rods, then back to short rods, and eventually back to spheres. The TEM results are not shown because they resemble the pictures in Figure 2. Furthermore, another test of the reversibility of the vesicle sizes started from 3.00 wt % of polymer in dioxane. The addition of 28 wt % water resulted in the formation of vesicles of 93.3 nm mean diameter (see Table 1). Addition of water to 40 wt % increased the size of the vesicles to 96.7 nm. A subsequent decrease in the water content to 28 wt % resulted in the decrease of the vesicle size to 87.6 nm. The difference in the vesicle size from 96 to 87 nm is of statistical significance at the 99% confidence level. Figure 4 gives plots of the vesicle sizes as a function of the polymer concentration for different water contents and also indicates the various concentration steps which were performed in the reversibility test. The error bars indicate the variation of the averages at the 95% confidence level. This experiment clearly demonstrates the reversibility of the vesicle sizes with changes in the water content and suggests that the vesicles are, indeed, equilibrium structures.

The electron microscopy investigation clearly shows that the aggregate morphologies are, indeed, reversible for the present system. However, the mechanisms of the forward and backward

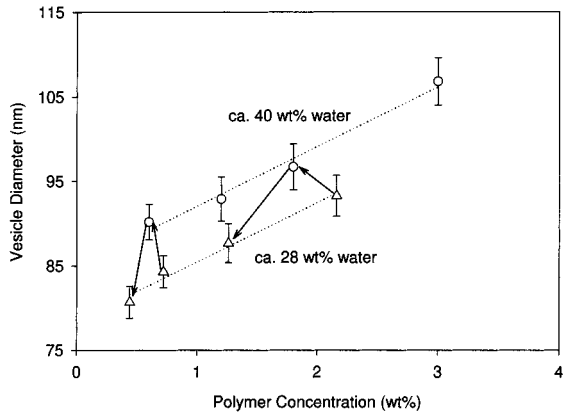

Figure 4. Vesicle sizes under various conditions. The arrows show the reversibility of vesicle sizes for two initial polymer concentrations. The error bars indicate the variation ranges of the average vesicle sizes at the 95% confidence level.

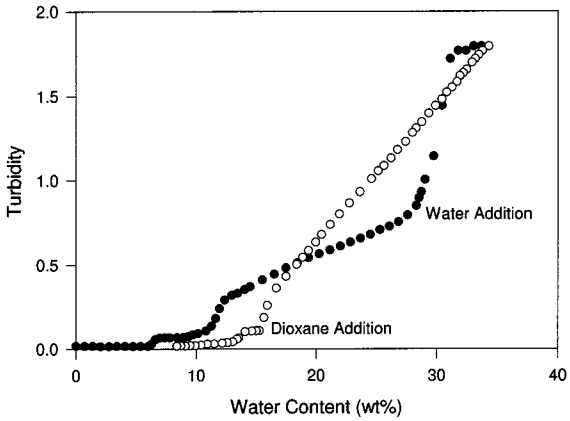

Figure 5. Morphological transitions examined by turbidity measurements for 1.00 wt % of the fractionated PS_{310}-*b*-PAA_{52} solution upon addition of water and subsequently addition of dioxane. The closed circles represent the addition of water, while the open ones reflect the reverse process upon addition of dioxane.

morphological transitions are probably different. Also, the kinetics of redistribution of aggregate sizes can be very slow for some cases. This aspect can be appreciated when one examines the results of turbidity measurements for the reversibility of the morphological transitions. Figure 5 shows a plot of the turbidity against the water content resulting from the addition of water to a 1.00 wt % fractionated PS_{310}-*b*-PAA_{52} solution to >30 wt % water and the subsequent addition of dioxane to reduce the water content back to <10 wt %. The variation of the turbidity upon water addition, represented by closed circles, shows three sharp jumps. These jumps are associated with three morphological transitions from single chains to spheres, from spheres to rods, and from rods to vesicles (see section 3.2.2). However, the reverse process (following the addition of dioxane) represented by the open circles only shows two sharp drops. Judging from the water contents and the polymer concentrations, these two drops correspond to the transitions from rods back to spheres and from spheres back to single chains. No sharp drop associated with the transition from vesicles to rods was found. The absence of the sharp discontinuity from vesicles back to rods suggests that the mechanism of vesicle to rod formation must be very different from rod to vesicle formation. It is essential to keep in mind that the vesicle to rod transformation does take place on dioxane addition, as is seen from TEM results. Also, it should be borne in mind that the polymer concentrations are considerably lower during the reverse process, as was discussed above.

In the studies of surfactant systems and block copolymers in bulk, a variation of temperature is frequently used to induce morphological transitions under equilibrium conditions.[17,38] This was also tried in the present system. However, it was found that even a change from room temperature to 90 °C did not produce an appreciable change in the turbidity, suggesting that no morphological change occurred. This experiment was performed on various aggregate solutions under different conditions, even at water contents close to the transition boundaries. None of the tests led to an observable turbidity change. After the temperature changes, TEM was employed to observe aggregate morphologies, and again no changes were seen. Thus, the aggregate morphologies of the PS-*b*-PAA/dioxane/water system are not very sensitive to temperature changes. However, the kinetics should accelerate appreciably with increasing temperature. Therefore, the aggregates should reach equilibrium more easily at the high temperature. The fact that aggregates are stable at high temperature also supports the argument that the morphologies observed represent true equilibria.

3.1.4. Thermodynamic Considerations. From the kinetic, stability, and reversibility tests, it is reasonable to draw the conclusion that in the present system the sizes and morphologies of the spheres, short rods, long rods, and small vesicles are thermodynamically controlled. However, it should be pointed out that it is generally accepted that in colloid systems spherical and long rodlike micelles can be equilibrium structrues,[1,25] while the equilibrium nature of the short rods and vesicles has been questioned.[25,36]

Most of previous studies in small molecule surfactants found that short rods are not thermodynamically stable due to high end-cap energies, which drive the short ones to form the equilibrated long-rod morphology.[25] The studies were performed on a single surfactant, which means that all molecules were of exactly the same structure. In the present system, the reversibility in the length of rods is clearly shown in parts B to C of Figure 2 and then to part H. Also, an increase in the temperature does not change the length of the rods despite the acceleration of kinetics. Thus, experimentally, it appears that the rod length is controlled by thermodynamic factors. Recent theoretical studies on mixed surfactant systems have shown that aggregates can possess different curvatures in different regions of the aggregates resulting from an uneven distribution of different molecules in the aggregates.[32−35] In a copolymer system, block copolymers are, effectively, a mixture of different chain lengths due to the polydispersity of the copolymer, even if the copolymer molecular weight has a narrow distribution.[53] For example, a polymer having an average of 100 repeat units and a polydispersity of 1.05 is, in fact, composed of a range of polymer chains from 0 to 200 repeat units, with only 1.8% of the chains having the average value.[53] Therefore, in the present study, when a rodlike morphology is favorable for a copolymer solution, a small portion of the copolymer chains from the longer end of the corona length distribution can selectively aggregate at the chain ends and thus stabilize the rod ends by minimizing the overall energy. Thus, because of the presence of a molecular weight distribution, short rods can be a thermodynamically stable morphology. A similar argument will be used later on for vesicles. Entropic factors probably also play a role in stabilizing the short-rod structure. As the water content increases, the driving force for rod formation increases and the concentration of long rods increases at the expense of both short rods and spheres.

The equilibrium nature of vesicles has been the subject of some controversy.[25,28−36] Recent arguments on the subject have been focused on the reversibility of the vesicular structrue.[36] In the present system, the reversibility of the vesicular morphology is confirmed from TEM results (see Figure 2, part D to E and then to F, and Table 1) and further supported by the invariance of the structure with temperature. Theoretically, as the water content reaches a region where a bilayer structure is favorable, the curvatures at two sides of the bilayers can differ due to the uneven distribution of different polymer chains. As the difference in the curvature reaches a sufficient value, the bilayer structure will fold spontaneously to a more favorable vesicular structure.[32] Another theoretical study showed that equilibrium vesicles should have a size polydispersity of 0.283, where the polydispersity is defined as the ratio of the relative standard deviation of the radius over the peak radius.[35] In the present study, defining polydispersity as the ratio of the standard deviation of the diameter over the average diameter, the vesicles have a polydispersity of 0.16−0.20, which are close to the theoretically calculated value. Additional evidence in favor of the equilibrium nature of the vesicles comes from the stability as well as the distribution of the vesicle sizes over time under conditions where the sizes are known to change in response to a change in the water content and temperature. Therefore, it is reasonable to conclude that these vesicles are true equilibrium structures.

3.2. Phase Diagrams of Fractionated and Unfractionated PS_{310}-*b*-PAA_{52} Copolymers. *3.2.1. Determination of Phase Diagrams.* The morphologies shown in the phase diagrams were determined from TEM pictures. For each copolymer, ca. 10 polymer concentrations from 0.1 to 10 wt % were examined. For each polymer concentration, the aggregate morphology was observed using TEM at ca. 10 consecutive water contents after the appearance of aggregates. Thus, ca. 100 points representing the various morphologies seen at different polymer concentrations and water contents were put on each graph. The boundaries for different morphologies (or phases) were determined by drawing smooth lines between the points representing different morphologies. Using the above method, the phase diagram for the fractionated copolymer was determined and is shown in Figure 6. Closed circles, plus signs, and open circles represent spheres, rods, and vesicles, respectively. Mixed symbols stand for the corresponding mixed morphologies. The solid lines are the boundaries determined from the TEM pictures, while the dotted line is the micellization curve determined from SLS measurements (see section 3.2.2). The upper graph (A) shows regions of stability on a plot of the logarithm of the polymer concentration against the water content. The lower graph (B) is a part of the classical ternary phase diagram. The polymer concentrations are corrected after each dilution resulting from water addition. Thus, the slope of a line connecting a family of points for every polymer concentration has a downward slope with increasing water content in both parts of the figure. Figure 7 shows the phase diagram of the unfractionated PS_{310}-*b*-PAA_{52}, which contains ca. 10 wt % homopolystyrene. For simplicity, the experimental points have been omitted. All the lines and symbols have the same meaning as those in Figure 6. It should be noted that no macrophase separation takes place under any conditions studied here, and only the microstructures of the aggregates change.

3.2.2. Boundaries of the Morphological Transitions. Several different methods, including SLS, DLS, and turbidity measurements, have been tried to determine morphological boundaries in addition to TEM, because light scattering techniques and

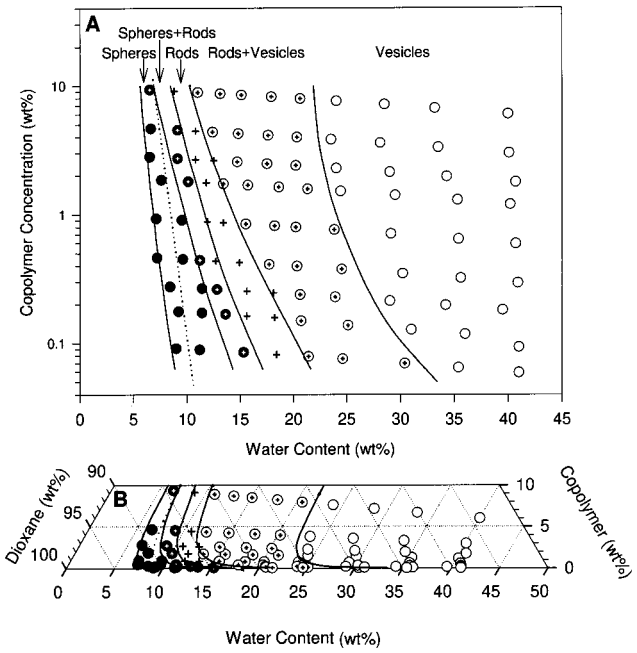

Figure 6. Phase diagram of the fractionated copolymer PS_{310}-*b*-PAA_{52} in dioxane/H_2O mixture. The symbols stand for morphologies, i.e., closed circles for spheres, closed circles with plus sign for mixtures of spheres and rods, plus sign for rods, open circles with plus sign for mixtures of rods and vesicles, open circles for vesicles. The solid lines are the phase boundaries determined from TEM pictures. The dotted line is the micellization curve from SLS measurements. (A) (top) shows the regions of stability on a plot of the logarithm of the polymer concentration against water content. (B) (bettom) is a part of a ternary phase diagram.

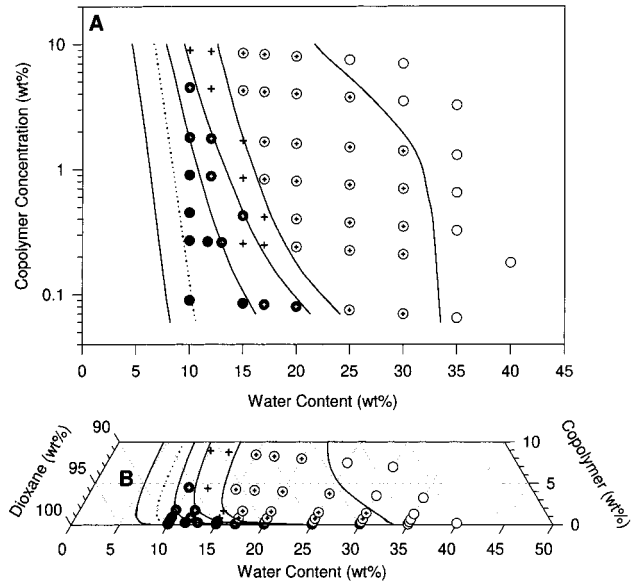

Figure 7. Phase diagram of the unfractionated copolymer PS_{310}-*b*-PAA_{52} in dioxane/H_2O mixture. All the symbols, lines, and graphs have the same meanings as those for Figure 6.

turbidity measurements have been used frequently in the past for studies of the micellization of block copolymers and morphological transitions of surfactant systems.[1,30] In our group, SLS measurements have been frequently used to determine cwc, which is defined as the critical water content at which micellization or aggregation takes place.[8−11] In the present study, cwc can be considered as the single-chain/sphere boundary, since spheres are the initial aggregate form. The results of SLS measurements are shown in Figure 8 as a plot of the scattered

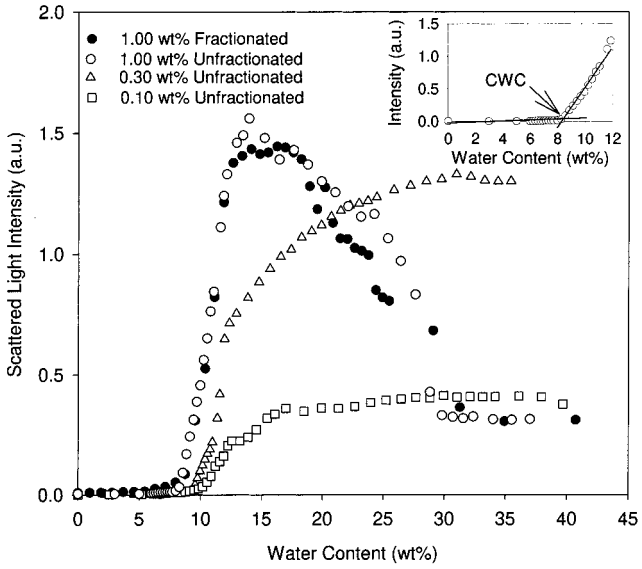

Figure 8. Plot of the scattered light intensity versus the water content for fractionated and unfractionated copolymer PS_{310}-*b*-PAA_{52}. The insert graph shows the determination of the cwc.

light intensity against the water content for fractionated and unfractionated PS_{310}-*b*-PAA_{52}. The closed circles represent the result for 1.00 wt % of the fractionated polymer, while open symbols indicate the curves of the unfractionated copolymer at various polymer concentrations. The initial jump is used to determine the cwc, as shown in the insert (upper right) of Figure 8.[8] The cwcs at different polymer concentrations can be used to determine the boundary between single chain and sphere regions in the phase diagram; the boundaries are drawn as dotted lines in Figures 6 and 7 for comparison with the results of TEM. These dotted lines do not coincide with the boundaries determined by TEM; the lack of coincidence is probably due to the difference in the detection sensitivity of different methods.[24]

As seen in Figure 8, for the curve of 0.10 wt % of the unfractionated copolymer (open squares), a second jump can be clearly seen from the scattered intensity. Judging from the jump position, ca. 14 wt % water, and comparing with Figure 7, the second jump is probably associated with the transition from spheres to rods. The curve of the 0.30 wt % polymer solution does not show a clear second jump before reaching a plateau at high water contents. By contrast, the curves of the 1.00 wt % polymer solutions (closed and open circles) have no second jumps at all; instead, they have a sharp drop before the plateau. The difference in the shapes of the curves at different polymer concentrations is due to the fact that both the size and the concentration of the particles influence the scattered intensity. When the aggregate sizes are too big or the concentration too high, interaggregate scattering will influence the final detected intensity, which leads to the complicated appearance of the curves seen here. Thus, the scattering curves cannot be simply linked to the morphological changes. DLS was also used to monitor the aggregate morphologies which appear on addition of water. Because of the complexity of the scattering profiles, only the morphological transition from single chains to aggregates can be determined clearly by that method. Since we are interested in various morphological transitions and DLS did not provide specific information about that aspect, DLS results will not be discussed in detail.

Turbidity measurements were also performed to determine the boundaries of the different morphologies in the present study.

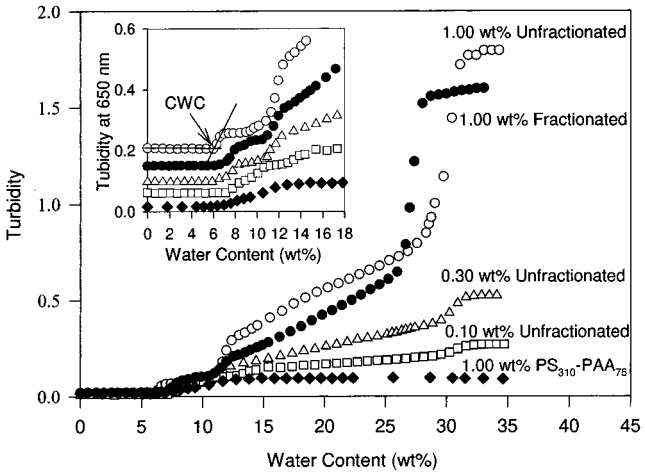

Figure 9. Plot of the turbidity against the water content for various samples. The insert shows an enlarged view of the curves at low water contents; the curves are shifted vertically relative to each other for the sake of clarity.

Figure 9 shows the plots of turbidity against the water content for fractionated and unfractionated copolymers at various polymer concentrations. Except for the closed diamonds which represent the data for the 1.00 wt % copolymer PS_{310}-*b*-PAA_{75} solution, all the other symbols have the same meanings as those given in Figure 8. The insert in Figure 9 shows an enlarged view of the curves at low water contents; the plots are shifted vertically relative to each other for the sake of clarity. The cwc is determined in the same way as those in SLS measurements, and is also shown in the insert of Figure 9 for the 1.00 wt % unfractionated sample. One can see that all the curves for the fractionated and unfractionated copolymer PS_{310}-*b*-PAA_{52} give three jumps for all polymer concentrations. The cwc values determined from turbidity measurements, i.e., 6.3, 7.0, and 7.8 wt % water for 1.00, 0.30, and 0.10 wt % unfractionated polymer solution, respectively, are in general agreement with the boundaries determined from TEM observation (see Figure 7). More importantly, the positions of the three jumps, i.e., 6.9, 11.5, and 26 wt % water for 1.00 wt % fractionated polymer solution, coincide closely with the transition from single chains to spheres, from spheres plus rods to pure rods, and from rods plus vesicles to vesicles in the phase diagrams (see Figure 6), respectively. This provides evidence, therefore, that the major changes occur on the high water content sides of morphological regions (rather than at low water content sides), i.e., at the sphere + rod/rod or rod + vesicle/vesicle transition.

Further confirmation of the correspondence between the jumps in turbidity and the morphological changes comes from experimental results of a fractionated copolymer PS_{310}-*b*-PAA_{75}. As can be seen in Figure 9, the plot for a 1.00 wt % PS_{310}-*b*-PAA_{75}, represented by closed diamonds, shows only one discontinuity at ca. 6.6 wt % water content, reflecting the formation of spherical micelles from single chains. Furthermore, TEM investigation of the aggregates at several water contents, e.g., 10 and 35 wt % water, confirms that only spherical micelles have been formed. The absence of the morphological transitions to rods and vesicles is reasonable in view of the PAA block length, which allows only spherical micelle formation. Turbidity measurements can, therefore, provide a very useful method for obtaining the approximate morphological boundaries.

3.2.3. Effect of the Water Content on the Aggregate Morphology. As seen from both phase diagrams (see Figures 6 and 7), as the water content increases, the polymer single chains first self-assemble to spherical aggregates, then to sphere and rod

mixtures, to rods, to rod and vesicle mixtures, and finally to vesicles, for all polymer concentrations. For example, 1.00 wt % fractionated copolymer chains in solution first aggregate to form spherical micelles at 9.5 wt % water; the spheres have an average radius of 13.6 nm with a standard deviation of 1.9 nm and have an average aggregation number of 180. As the water content increases, the spheres change to a mixture of spheres and short rods at 10.9 wt % water. As the water content increases further, the relative number of spheres decreases until only rods are seen at 13.4 wt % water. Morphologies then change to a mixture of rods and vesicles at 20 wt % water. Again, as the water content increases, the number of vesicles increases until pure vesicles are seen at 40 wt % water. Further addition of water does not change the aggregate morphology.

The morphological changes with increasing water content can be attributed to the change of the solvent quality toward both blocks of the copolymer. As the solvent becomes poorer for the core-forming PS block with increasing water content, the interfacial tension increases, while the corona repulsion may not change much since both dioxane and water are good solvents for the corona-forming PAA block. Thus, larger spherical aggregates tend to form to minimize the total interfacial energy. However, in the process of the core enlargement, the stretching of polymer chains in the core increases, which causes an increase in that component of the free energy which reflects core chain stretching. When the stretching is too high, an aggregate has to adapt another geometry to relax the stretching, and thus the total free energy is minimized. As a result, rodlike aggregates appear. As the water content continues to increase, the rods can grow to significant length because of the interplay of the interfacial tension and the corona repulsion with contributions from the high end-cap energy.[25] However, the copolymer rods cannot grow to infinite length due to the new balance of interfacial tension, corona repulsion, and stretching, as well as the uneven distribution of polymer chains in the rods and entropic factors related to the number of particles. Thus, the diameter of the rods increases upon further addition of water and core chain stretching is building up again. Similar to the change from spheres to rods, the rod to bilayer transition is also a result of easing the stretching of polymer chains in the core (see discussion in section 3.1.4). Overall, the aggregate morphology always changes in a direction that decreases the overall free energy, which, in the present system, is from spheres to short rods, then to long rods, and finally to vesicles with increasing water content. If more water is added into the system, the aggregate should grow further until the vesicles are no longer stable. Therefore, inverted structures should appear. In the present system, however, the morphology does not change further beyond the vesicular structure because the chain mobility is frozen at high water contents, i.e., above ca. 40 wt %. The inverted structure can be observed for copolymers with shorter PS block lengths, which increase chain mobility at high water contents.[54] It is noteworthy that, as the water content increases after the formation of aggregates, the viscosity of the aggregate solution progressively increases, first due to the change of spheres to short rods and then to long rods, but then decreases because of the transition from rods to vesicles.

3.2.4. Effect of the Polymer Concentration on the Aggregate Morphology. In the preceding section, we have explored the effect of the water content on the morphology. We now discuss the effect of polymer concentration. As seen from Figures 6A and 7B, the slopes of morphological boundary lines are generally from upper left to lower right. Therefore, with increasing polymer concentration, the aggregate morphology tends to change in a manner similar to the effect of increasing water content. The pattern of morphological transitions can vary depending on the water content. For example, at 15 wt % water (see Figure 6), the aggregates change from spheres to spheres plus rods, to rods, and then to rods plus vesicles. On the other hand, at 25 wt % water, the aggregates change only from rods plus vesicles to pure vesicles over the polymer concentration region studied here. The trend of the boundary lines is, at least, partly due to the change in the solvent composition with changing polymer concentration. Starting at low polymer concentrations, as the polymer concentration increases, the water-to-dioxane ratio also increases. As expected, the aggregate morphology goes through a general transition from spheres to rods and then to vesicles, which is similar to that of increasing water content. Other factors, such as pure polymer concentration effect, may also contribute to the shape of the boundaries.

TABLE 2: Effect of the Polymer Concentration on the Vesicle Size

polymer (wt %)	0.6	1.2	1.8	3.0	5.0
water/dioxane (wt %/wt %)	40/59.4	40/58.8	40/58.2	40/57	40/55
mean diameter (nm)	90.2	92.9	96.7	106.8	123.7
std. dev. (nm)	14.8	18.4	18.9	20.1	70.1
95% conf. (nm)	2.1	2.6	2.7	2.8	9.9
99% conf. (nm)	2.7	3.4	3.4	3.7	12.9
mean wall thickness (nm)	27.0	27.1	27.2	27.2	27.2
std. dev. (nm)	3.0	2.7	3.2	3.2	2.5
95% conf. (nm)	0.4	0.4	0.4	0.4	0.3
99% conf. (nm)	0.6	0.5	0.6	0.6	0.4
std. dev./mean dia.	0.16	0.20	0.20	0.19	0.57

It is of interest to compare the vesicle sizes at the same water content as a function of polymer concentration. Table 2 lists statistical results on the vesicles from TEM pictures at ca. 40 wt % water with various polymer concentrations. The results are based on a population of 200 and the polymer concentration is corrected for dilution. One can see that the outside diameters of the vesicles increase gradually between 0.6 and 3.0 wt % (see also Figure 4), but increase more steeply between 3.0 and 5.0 wt %. The difference in vesicle sizes is statistically significance above the 95% confidence level, as seen in Table 2. The wall thickness is similar under all conditions, while the polydispersities of the vesicles are narrow at and below 3.0 wt % but are high at 5.0 wt %. At 5.0 wt % polymer, one sees very large multilayer vesicles appearing instead of only small unilamellar vesicles; the multilayer vesicles will be discussed in the next paragraph. In the solution, it is possible to obtain approximate vesicle sizes from DLS measurements by treating them as spheres.[55] Using the CONTIN method,[55] the *z* average hydrodynamic radius can be obtained for various polymer concentrations at the same water content, ca. 40 wt %. The result is shown in Figure 10 by plotting the inverse hydrodynamic radius against the polymer concentration. The hydrodynamic radius (R_{h0}) extrapolated to zero polymer concentration is ca. 450 nm, which is significantly larger than the size measured by TEM. Although DLS measurements give *z* average values and the fact that the corona stretching in solution contributes to the sizes of the hydrodynamic radii, the difference between R_{h0} from DLS and the radius from TEM is too high to be accounted for by these terms only. Other factors must also contribute to the high values of the hydrodynamic radii.

Some unusual phenomena are encountered at high polymer concentrations. Figure 11 shows the aggregates formed from 10 wt % polymer solution. At 13 wt % water, regularly arranged rods appear, as shown in Figure 11A. Also, the viscosity of the aggregate solution is very high at this point. If the solution container is inverted, several hours are needed for the solution

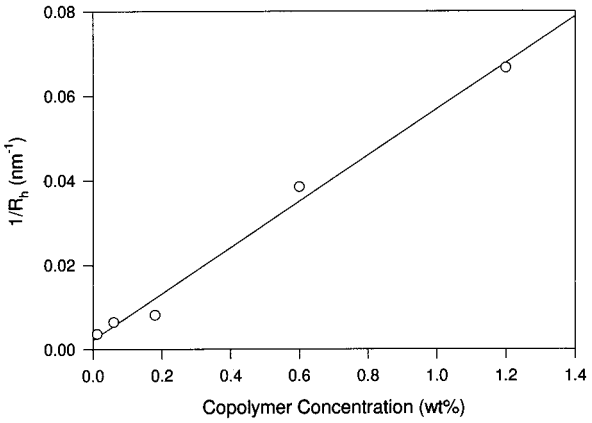

Figure 10. Plot of the reverse hydrodynamic radii versus the polymer concentration.

to flow to the other end. This highly viscous rod solution behaves like a soft-gel. This behavior could be due to the formation of an ordered structure, i.e., hexagonally packed rods. Figure 11B shows a multiple-layer vesicle at 40 wt % water. This type of aggregate is responsible for the high polydispersity seen for the vesicles. This multilayer vesicle could be the result of fusion and foraging of the overcrowded unilamellar vesicles.[31,56]

3.2.5. Effect of the Fractionation on Morphological Boundaries. A comparison of Figures 6 and 7 shows similarities of the phase diagrams of fractionated and unfractionated copolymers. Both exhibit the same number and the same types of morphologies and go through the same phase transition processes, i.e., from sphere to rod and then to vesicle. Generally, the shapes of the morphological boundaries are similar. There are two main differences. First, the line characterizing the onset of the spherical aggregate formation in the phase diagram of the unfractionated copolymer lies at lower water contents than that of the fractionated diblock. This is obviously due to the presence of homopolystyrene (ca. 10 wt %), which is less soluble than the diblock and thus induces the formation of aggregates at lower water contents.[8] Second, the boundaries of the other morphological transitions shift to higher water contents. The dissolution of homopolystyrene into the core of the aggregates eases the stretching in the core and thus shifts the morphological transitions to higher water contents. Additionally, in the phase diagram of the unfractionated polymer, the rod + vesicle/vesicle boundary curves to the right (see Figure 7A), while the lines for rest of the morphological boundaries curve to the left. The reason for the difference in shape is not clear.

3.3. Pathways of the Morphological Transitions. Before starting the discussion on the pathways of the morphological transitions, it is important to know the fractions of single chains and aggregates in solution as a function of the water content. Figure 12 shows the plot of the cwc versus the logarithm of the copolymer concentration. The cwcs for fractionated (closed symbols) and unfractionated (open symbols) copolymers are obtained from both SLS (circles) and turbidity (triangles) measurements. The method used in the determination of the cwc was illustrated in Figures 8 and 9. All the plots can be fitted to straight lines with $r^2 > 0.99$. The polymer concentrations are corrected for dilution upon addition of water. Duplicate runs are shown for the unfractionated samples studied by SLS (open circles) to illustrate reproducibility.

It is noted that the turbidity measurements give lower cwc's than SLS measurements. The difference is probably due to the high detection sensitivity of the turbidity measurement for the present system. The slopes of the plots obtained from both

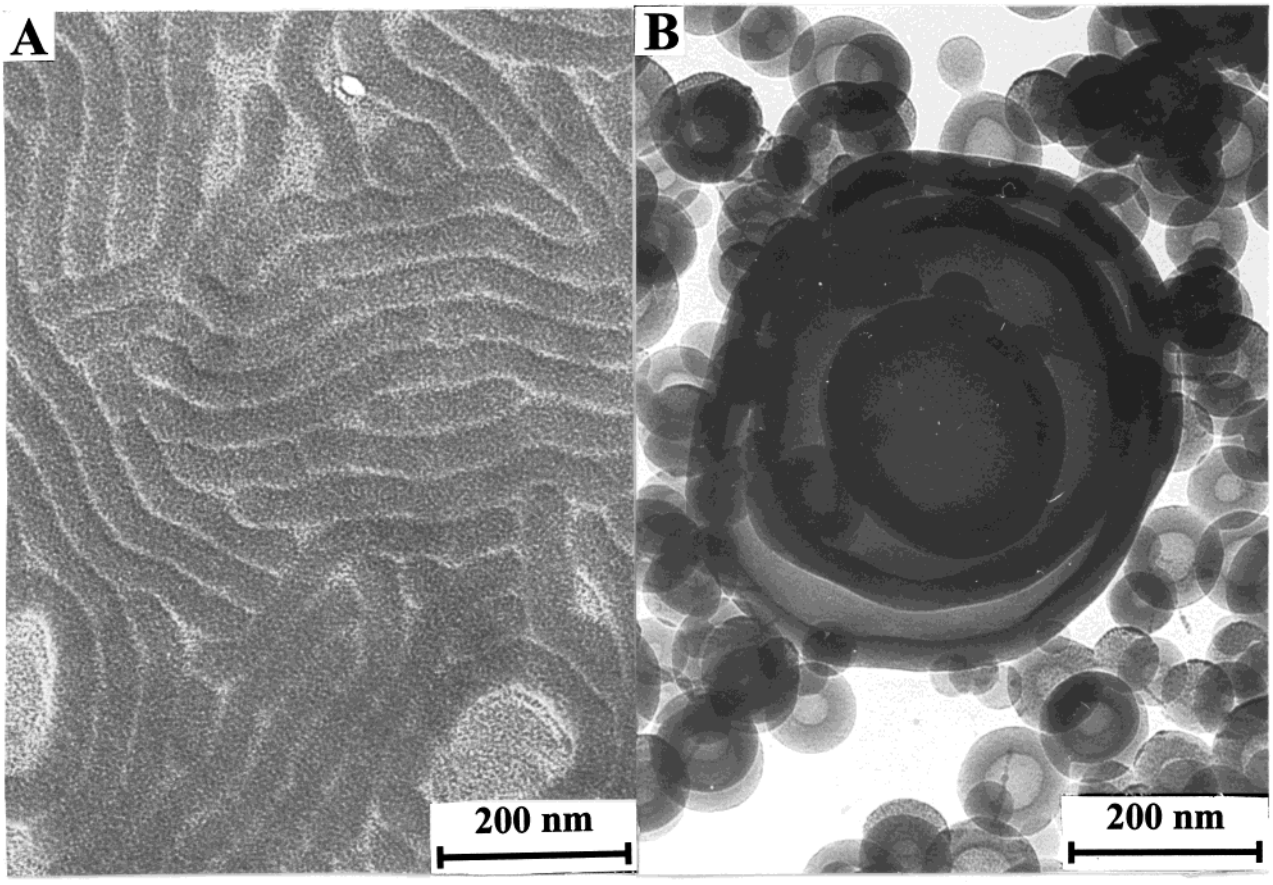

Figure 11. Morphologies for a 10 wt % fractionated copolymer PS_{310}-*b*-PAA_{52} in dioxane at two water contents: (A) 14 wt %; (B) 40 wt %.

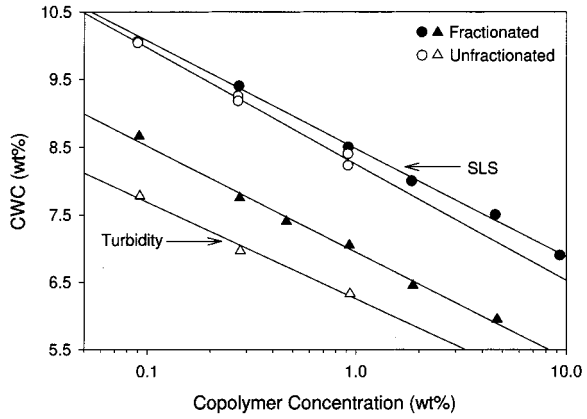

Figure 12. Plot of the cwc against the logarithm of the polymer concentration for fractionated and unfractionated PS_{310}-*b*-PAA_{52} using SLS and turbidity measurements.

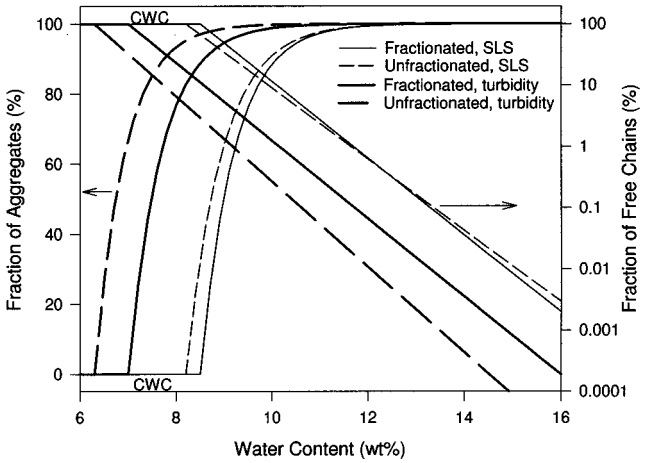

Figure 13. Plots of the fraction of aggregates and fraction of free chains against the water content for 1.00 wt % fractionated and unfractionated PS_{310}-*b*-PAA_{52} copolymer from both SLS and turbidity measurements.

methods are similar for the fractionated sample. The plots of the unfractionated polymer have slightly different slopes, which is probably due to the presence of the homopolymer. Using previously developed formalism,[8] the fraction of the aggregates $[(C - \mathrm{cmc})/C]$ in the total copolymer can be obtained from the following equation:

$$(C - \mathrm{cmc})/C = 1 - \exp[-2.303([H_2O] - \mathrm{cwc})/b] \quad (1)$$

where C is the total polymer concentration after the correction, cmc is the critical micellization concentration, $[H_2O]$ represents the water content, and b is the slope obtained from Figure 12. The fraction of the single chains in the total copolymer is 1 minus the fraction of aggregates in the total copolymer.

Thus, the fraction of aggregates and of single chains in the polymer solution can be calculated as a function of the water content. Figure 13 shows plots of the fractions of single chains and aggregates as a function of the water content for 1.00 wt % fractionated and unfractionated copolymers. Since a higher cwc results in a higher fraction of single chains, the results from SLS measurements will give higher fractions of single chains. For example, at 10 wt % of water, either ca. 1 or ca. 10 wt % of single chains are present in the solution, depending on whether one uses turbidity or SLS measurements. At 15 wt % water, either only 0.0001 or only 0.01% of polymer chains are in the single chain state. Also, the chain dynamics should be a function of the water content, as discussed in section 3.1.1. Thus, the single chains should be able to make some contribution to the aggregation processes at low water contents, but probably have a negligible effect at relatively high water contents, i.e., above ca. 15 wt %.

Since the contribution of single chains to the aggregation is a function of the water content and the aggregate morphology changes with increasing water content, the contribution varies for different morphological transitions. For the formation of spheres at the onset of the aggregation, single chains should make the major contribution to aggregation process, although the collision/fusion of nonequilibrium spheres may also contribute. As the water content increases, the collision/fusion of nonequilibrium aggregates becomes important for the formation of short rods, with single chains playing a minor role. In the growth of short rods to long rods, the transition is dominated by the rate of the collision and fusion since the water content is relatively high, i.e., 13 wt %. The single chain involvement in the formation of vesicles probably is negligible since the water content is high. The following paper will discuss the formation of vesicles from rods in detail.[51]

3.4. Estimation of Thermodynamic Functions on the Basis of the Morphological Boundaries. *3.4.1. Theoretical Aspects.* The formation of spheres in the present system is considered to follow the closed association model. Similar to the previous thermodynamic study,[50] the free energy for the transfer of 1 mol of polymer single chains into the spherical core (ΔG_S) can be estimated.

$$\Delta G_S = RT \ln(\mathrm{cmc}) \quad (2)$$

cmc is the critical micellization concentration of polymer chains for sphere formation in moles per liter. In the present study, cwc is frequently measured because the study was performed by changing water content instead of the polymer concentration. The total polymer concentration (C), after the correction for water addition, is equal to the cmc at the cwc. Thus,

$$\Delta G_S = RT \ln(C) \quad (3)$$

Because the ΔG_S involves the transfer of 1 mol of single chains and the equilibrium constant (K_S) refers to the formation of 1 mol of spherical aggregates, the equilibrium constant for sphere formation can be estimated.

$$K_S = C^{-N_S} \quad (4)$$

N_S is the aggregation number of the spheres, which can be estimated from TEM pictures.

Since the rods constitute a mixture of short and long rods, it is too difficult to estimate thermodynamic functions for each rod length. As an approximation, all the rods are considered to be of the same (average) size and the formation of rods from spheres is considered as a one-step process. Thus, rod formation can be expressed as

$$(N_R/N_S)S \overset{K_{SR}}{\rightleftharpoons} R \quad (5)$$

N_R is the average aggregation number of the rods, and K_{SR} is the sphere-to-rod equilibrium constant. If C_S and [R] represent the critical concentration of spheres for rod formation and the rod concentration, respectively, the free energy of transforming 1 mol of spheres in solution to rods ($\Delta G_{SR}'$) can be estimated using

$$\Delta G_{SR}' = -RT \ln(K_{SR})/(N_R/N_S) = RT \ln(C_S) - \mathrm{RT} \ln([\mathrm{R}])/(N_R/N_S) \quad (6)$$

If the aggregation number is high, the second term is small and can be neglected. $\Delta G_{SR}'$ can then be estimated by omitting the second term.

$$\Delta G_{SR}' \approx RT \ln(C_S) \quad (7)$$

Because $\Delta G_{SR}'$ is related to transfer of 1 mol of spheres, the free energy of transferring 1 mol of single chains from spheres to rods (ΔG_{SR}) is then equal to the value of $\Delta G_{SR}'$ divided by the aggregation number of the spheres (N_S). If the initial sphere concentration can be represented as C/N_S, the C_S can be replaced by C/N_S at the critical water content for rod formation. Thus,

$$\Delta G_{SR} = (RT/N_S) \ln(C_S) = (RT/N_S) \ln(C/N_S) \quad (8)$$

On the basis of eqs 6 and 8, one may also estimate the K_{SR}, which refers to the formation of 1 mol of rods.

$$K_{SR} = (C/N_S)^{-N_R/N_S} \quad (9)$$

Following the simplified method developed for the rod formation, the free energy of transferring 1 mol of single chains from rods to vesicles (ΔG_{RV}) and the equilibrium constant for the transition form rods to vesicles (K_{RV}) with an aggregation number of N_V can be roughly estimated as follows:

$$\Delta G_{RV} = -(RT/N_V) \ln K_{RV} \approx (RT/N_R) \ln(C/N_R) \quad (10)$$

$$K_{RV} = (C/N_R)^{-N_V/N_R} \quad (11)$$

The estimates for rod formation and vesicle formation contain more uncertainties than those for sphere formation, but they are intended to show the trends; the values obtained for rod and vesicle formation should, therefore, not be considered as accurate estimates.

The free energies obtained under equilibrium conditions are all state functions. Thus, the free energies of transferring 1 mol of single chains from solution to rods (ΔG_R) and to vesicles (ΔG_V) can be obtained, respectively, from:

$$\Delta G_R = \Delta G_S + \Delta G_{SR} \quad (12)$$

$$\Delta G_V = \Delta G_R + \Delta G_{RV} = \Delta G_S + \Delta G_{SR} + \Delta G_{RV} \quad (13)$$

3.4.2. Estimated Parameters. The thermodynamic functions can now be roughly estimated using eqs 3, 4, and 8−13. The aggregation numbers for spheres, rods, and vesicles are estimated to be 180 from Figure 2A, 2400 from Figure 2B,[57] and 5000 from Figure 2D, respectively. Since the single-chain/sphere, sphere + rod/rod, and rod + vesicle/vesicle boundaries in the morphological phase diagrams (see Figures 6 and 7) correspond to the three major changes from single chains to spheres, from spheres to rods, and from rods to vesicles, these three boundaries are used to estimate thermodynamic functions. Figure 14 shows the free energies of transferring 1 mol of single chains to spheres, to rods, and to vesicles as a function of water content at 25 °C. It should be kept in mind that the values of the free energies and the regions of morphological transitions from spheres to rods and from rods to vesicles are only estimates. However, the graph definitely shows the trends of these changes. As the water content increases from ca. 5 to ca. 10 wt %, the free energy of the sphere formation decreases. Rods then become the lowest energy morphology between ca. 10 wt % and ca. 18 wt %. At higher water contents, vesicles become thermodynamically most stable. The logarithms of equilibrium constants for sphere formation are ca. 450−850 at 25 °C, much higher than those for small molecule surfactants (65−478).[24] The formation of rods and vesicles involves relatively lower logarithm values, i.e., 65−95 for the rod formation from spheres and 12−18 for the vesicle formation from rods. The major morphology present in solution depends on the relative values of three equilibrium constants. For example, with addition of water, only spheres are present initially because of the high K_S values. As the water content increases, coexistence regions are encountered. The relative widths of these regions for the various mixtures of morphologies are undoubtedly related to the relative magnitudes of the equilibrium constants. Thus, the narrowness of the sphere + rod region relative to the wide range of the rod + vesicle region is dependent on the logarithm values of equilibrium constants, i.e., 65−90 for rods versus 12−18 for vesicles.

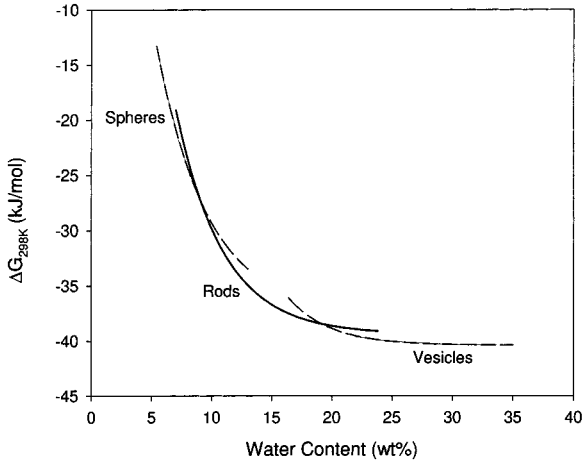

Figure 14. Estimates of the free energies of formation of various morphologies from single chains as a function of the water content.

3.5. Comparison to Other Systems. It is instructive to compare and contrast the morphological phase diagrams obtained in the present study with those of block copolymers in bulk, with small molecule surfactants in solution, and with PEO based copolymers in concentrated solution. The results for those three families of materials are most relevant to the present study.

3.5.1. Block Copolymers in Bulk. In the study of equilibrated phases in bulk, to overcome kinetic barriers, melted samples are annealed at high temperature for several minutes to several hours to achieve equilibrium and are then quenched to a low temperature.[17] The morphologies at that temperature are preserved and can be studied using TEM, SAXS, or other tools. However, careful handling of the samples, e.g., the length of the annealing time and the quenching speed, is needed to avoid the misidentification of the equilibrium phases.[22] In the present study, the aggregate solution was prepared by adding water progressively to the polymer solution and storing the samples for several days to allow them to reach equilibrium at each water addition interval; finally, the samples were quenched to liquid nitrogen temperature and freeze-dried to preserve the morphologies in solution. As will be seen in the subsequent paper, equilibration times under the conditions of the present study are of the order of several minutes. The present study thus utilizes a similar strategy to that used in the bulk studies, with precautions which include the use of small water content increments and very long annealing times relative to the equilibration times. More importantly, reversibility tests were

performed for each morphological transition to make sure that kinetics does not perturb the identification of equilibrium phases.

The phase behavior of diblock copolymers in bulk is characterized by the segregation term χN and the volume fraction *f*. *N* is the total number of repeat units in the copolymer and χ is the Flory−Huggins segment−segment interaction parameter, which decreases with increasing temperature. A model system, PS−PI, has been studied extensively.[17−22] In the strong segregation region ($\chi N \gg 10$), the sequence of microstructures or morphologies, as f_{PI} increases from 0 to 0.5, involves the following: disordered, Sphere, HEX, Gyroid, and LAM phases. A metastable phase, HPL, is located between Gyroid and LAM, while another unstable phase, OBDD, is also found near the Gyriod region. As f_{PI} increases from 0.5 to 1, a mirror image of the phases appears with inverted structures. The ordered phase transitioning from Sphere to HEX and then to LAM as f_{PI} increases from 0 to 0.5 is similar to the morphological changes seen in the present study, i.e., from spheres to rods and then to vesicles, with increasing water content. Thus, an increase in the water content has the same effect as an increase in the fraction or the length of the core-forming block (i.e., PS). In the bulk system, with increasing χN, the sequence of phase transitions depends on the starting volume fraction. For example, the phase sequence changes from disordered to Gyroid to HPL and then to LAM at a f_{PI} of 0.65, while at a f_{PI} of 0.69, it changes from disordered to HEX to Gyroid. The effect of increasing χN by decreasing temperature in the bulk resembles the polymer concentration effect in the present study. As the polymer concentration increases at different water contents, the morphologies go through different transition sequences, as discussed in section 3.2.4.

In the present study, the various morphologies appear only in the disordered state instead of in the ordered phase in bulk because the present study was performed at low polymer concentrations. However, at a relatively high polymer concentration, i.e., 10 wt %, we do have an indication of the appearance of ordered phases (see section 3.2.4). Also, we have observed ordered phases such as the HHH morphology before.[9] For the bilayer morphology, closed lamellae or vesicles are seen in the present study instead of only open lamellae in bulk. In the present system, many variables influence the phase behavior, while only two parameters control the phase behavior in bulk. Furthermore, various morphologies are seen to coexist at equilibrium in the present study, while this aspect has not been explored extensively in bulk. Also, in the present system, various morphologies can be formed simply by varying the water content for one copolymer, while a series of copolymer samples have to be synthesized to achieve the same purpose in bulk. Finally, since the aggregates in the present system can be prepared in liquid solution, including pure water, individual stable free-standing nanostructures of various morphologies can be isolated and studied individually. This opens up the opportunity for various applications, such as in drug delivery.[15,58]

3.5.2. Small Molecule Surfactant Systems. Aggregates of various morphologies can be easily obtained in both disordered and ordered phases from small molecule surfactant systems.[23−27] In addition to the phase transitions observed in ordered phases, which are similar to those in bulk copolymers, various morphologies also appear in the disordered micellar phases (L_1 and L_2). With increasing surfactant concentration or decreasing curvature energy, aggregates can change from spheres to rods and to bilayers before going to the ordered phases in a two-component system.[27] Different morphologies can be bypassed depending on the starting conditions. The effect of increasing surfactant concentration is parallel to that of increasing copolymer concentration in the present study, while the effect of decreasing curvature is similar to that of the water addition.

In the surfactant/water/oil ternary system, with the addition of water, aggregates may change from ordered phases to irregular bicontinuous structures to cylindrical micelles and then to spherical micelles, or from ordered phases to cylindrical micelles and then to spherical micelles, depending on the initial surfactant concentration in the oil.[23,26] Two different but complementary approaches can be invoked. Because water and oil have opposite effects on small molecule surfactants, both the interfacial tension and corona repulsion increase upon addition of water. As a result, the increase in the corona repulsion, which is dominant, drives the aggregates to change in a direction of bilayers to spheres. Another approach, which considers the effect of the volume fraction, can also explain the morphological changes. With increasing water content, the volume of the water (or hydrophilic) phase increases and the volume of the oil (or hydrophobic) phase decreases. Thus, the aggregates change from bilayers at low water contents to spheres at the high water contents. In our study, with increasing water content, the trend of the morphological transition is opposite to that in small molecule surfactant systems, i.e., from spheres to rods and then to vesicles (bilayers). Because dioxane is a common solvent for both blocks, corona effects do not contribute materially with increasing water content and only the interfacial tension increases appreciably. Therefore, aggregates change in the direction of spheres to bilayers (see discussion in section 3.1.4).

Vesicles can be present as a disordered phase in mixed surfactant systems.[28−30] With changing composition or concentration of the surfactant mixtures, pure spherical, rodlike, and vesicular morphologies or mixed morphologies can occur in the disordered phase, similar to the situation in the present study. Also, in the rod region, the aggregate solution is viscous. Since most surfactants have 12−18 carbons, the wall thickness of the vesicles cannot be varied over a wide range. By contrast, in the present system, because the PS block can change over a wide range of repeat units (the range from 100 to 1000 is easily accessible), the wall thickness can be varied over a broad range. In addition, the various aggregates in surfactant solution can be observed using freeze-fracture TEM, which can preserve the aggregate morphologies. This is similar to the method used to observe equilibrated morphologies in the present study. However, in the copolymer systems, it is easy to find regions of slow kinetics and then isolate the various aggregates for some applications.[15,58]

3.5.3. PEO based Copolymers in Concentrated Solutions. The PEO based copolymer systems, e.g., PPO-*b*-PEO and PBO-*b*-PEO, have relatively high molecular weights, and their kinetics can be slow or fast, depending on the experimental conditions.[1] Thus, PEO systems are more like the present system. For the PEO systems, aggregate solutions were monitored for weeks or months to see whether they reached equilibria.[38,42] In the present study, representative spherical, rodlike, and vesicular aggregate solutions have been examined for 14−24 month periods. It was found that, after the first few minutes or hours, the aggregate solutions had already reached equilibrium. Additionally, the reversibility of the morphological transitions was also examined for the present system.

In the PEO based copolymer systems, various morphologies appear only at relatively high polymer concentrations, i.e., above 20 wt %, as well as in the ordered phases for both two- and three-component systems.[37−43] In a PPO-*b*-PEO/water system, the phase sequence can go through L_1 (disordered phase) to I_1

(cubic) to H_1 (hexagonal) and then to L_α (lamellar) with increasing polymer concentration or increasing temperature.[38] In a PPO-*b*-PEO/water/oil ternary system, along the water to copolymer and then copolymer to oil sides, the phase can change from L_1 to I_1 to H_1 to V_1 to L_α and then to V_2 to H_2 to I_2 to L_2.[43] In the above studies, the phase transitions can be simply ascribed to the changes in the volume fraction of the oil phase or water phase.[42] In the present study, different effects can be responsible for the various morphological transitions. So far, all the morphologies which were seen in the PEO-based copolymer systems were detected by indirect methods, and no direct observation (e.g., using TEM) of these morphologies has been reported to our knowledge. In the PEO system, oil is generally used as a good solvent for the PPO block but a precipitant for the PEO block, while water is a good solvent for the PEO block but a precipitant for the PPO block. Our system, so far, has been studied only in mixtures of a common solvent and a precipitant for the PS block. Thus, macrophase separation can be seen in the PEO systems, but cannot be observed in our system.

4. Conclusion

The morphological phase diagrams of self-assembled nanoaggregates of the fractionated and unfractionated copolymer PS_{310}-*b*-PAA_{52} in dioxane/water have been determined. The morphological transitions occur at low polymer concentrations (0.1−10 wt % polymer) and relatively low water contents (0 to 45 wt % water). The morphologies encountered are in the order of spheres, rods, and vesicles. On the basis of the reversibility of both the morphology and size of aggregates as a function of the water content, it is suggested that the various observed morphologies, including vesicles, are true equilibrated thermodynamic morphologies.

With increasing water content, the block copolymers always form spheres first, then change to a mixture of spheres and rods, to rods, to a mixture of rods and vesicles, and finally turn to vesicles at all polymer concentrations. The mixtures of morphologies are also shown to be thermodynamically controlled since identical mixtures can be obtained starting with pure morphologies. For example, a mixture of spheres and rods can be obtained by increasing water content of pure spheres or decreasing water content of pure rods. Morphologies also change as a function of the copolymer concentration, generally in the direction of spheres to rods and to vesicles, although not all the morphologies are accessible for all the water contents. The fractionation moves the single-chain/sphere boundary to higher water contents for the fractionated copolymer in comparison to the unfractionated copolymer, but moves other phase boundaries to lower water contents. From the positions of the morphological boundaries, the thermodynamic functions of the morphological transitions are estimated and the corresponding equilibrium constants are also calculated.

The present phase diagram is compared with those of copolymers in bulk, small molecule surfactants in solution, and PEO based copolymers in solution. The effect of the volume fraction on the aggregate morphology for the present system is opposite to those of small molecule surfactant systems in the disordered phase and of the three comparison systems in the ordered phase. The other significant difference is that in the present system the various morphologies present in the disordered phase are observed directly using TEM. The direct observation of the equilibrated aggregates benefits from the freeze-drying technique and the fact that dioxane has high freezing point (near that of water) so that even mixtures of the two still have a significant vapor pressure at their freezing points. A combination of the freeze-drying TEM and turbidity measurements has proven to be very helpful in the investigation of various aggregates of block copolymers in solution in the present study.

Acknowledgment. We thank Dr. Lifeng Zhang for many helpful discussions and acknowledge the donors of the Petroleum Research Fund, administered by the American Chemical Society, for the support of this work.

References and Notes

(1) Tuzar, Z.; Kratochvil, P. *Adv. Colloid Interface Sci.* **1976**, *6*, 201. Tuzar, Z.; Kratochvil, P. In *Surface and Colloid Science*; Matijievic, E., Ed.; Plenum Press: New York, 1993; Vol. 15, p 1. Price, C. In *Developments in block copolymers*; Goodman, I., Ed.; Applied Science Publishers: London, 1982; Vol. 1, p 39. Selb, J.; Gallot, Y. In *Developments in block copolymers*; Goodman, I., Ed.; Applied Science Publishers: London, 1985; Vol. 2, p 27. Riess, G.; Hurtrez, G.; Bahadur, P. *Encyclopedia of Polymer Science and Engineering*, 2nd ed.; Wiley: New York, 1985; Vol. 2, p 324.

(2) Zhou, Z.; Chu, B. *Macromolecules* **1988**, *21*, 2548. Antonietti, M.; Heinz, S.; Schmidt, M.; Rosenaner, C. *Macromolecules* **1994**, *27*, 3276.

(3) Price, C. *Pure Appl. Chem.* **1983**, *55*, 1563. Gast, A. P.; Vinson, P. K.; Cogan-Farinas, K. A. *Macromolecules* **1993**, *26*, 1774.

(4) Halperin, A.; Tirrell, M.; Lodge, T. P. *Adv. Polym. Sci.* **1992**, *100*, 31.

(5) Gao, Z.; Varshney, S. K.; Wong, S.; Eisenberg, A. *Macromolecules* **1994**, *27*, 7923. Honda, C.; Sakaki, K.; Nose, T. *Polymer* **1994**, *35*, 5309.

(6) Zhang, L.; Eisenberg, A. *Science* **1995**, *268*, 1728. *J. Am. Chem. Soc.* **1996**, *118*, 3168.

(7) Zhang, L.; Yu, K.; Eisenberg, A. *Science* **1996**, *272*, 1777. Zhang, L.; Eisenberg, A. *Macromolecules* **1996**, *29*, 8805.

(8) Zhang, L.; Shen, H.; Eisenberg, A. *Macromolecules* **1997**, *30*, 1001.

(9) Zhang, L.; Bartels, C.; Yu, Y.; Shen, H.; Eisenberg, A. *Phys. Rev. Lett.* **1997**, *79*, 5034.

(10) Yu, Y.; Eisenberg, A. *J. Am. Chem. Soc.* **1997**, *119*, 8383. Yu, Y.; Zhang, L.; Eisenberg, A. *Macromolecules* **1998**, *31*, 1144.

(11) Zhang, L.; Eisenberg, A. *Polym. Adv. Technol.* **1998**, *9*, 677.

(12) Desbaumes, L.; Eisenberg, A. *Langmuir* **1999**, *15*, 36.

(13) Yu, K.; Eisenberg, A. *Macromolecules* **1996**, *29*, 6359. Yu, K.; Bartels, C.; Eisenberg, A. *Macromolecules* **1998**, *31*, 9399.

(14) Massey, J.; Power, K. N.; Manners, I.; Winnik, M. A. *J. Am. Chem. Soc.* **1998**, *120*, 9533.

(15) Guo, A.; Liu, G.; Tao, J. *Macromolecules* **1996**, *29*, 2487. Ding, J.; Liu, G. *Macromolecules* **1997**, *30*, 655. Henselwood, F.; Liu, G. *Macromolecules* **1998**, *31*, 4213. Ding, J.; Liu, G. *J. Phys. Chem. B* **1998**, *102*, 6107.

(16) Spatz, J. P.; Mössmer, S.; Möller, M. *Angew. Chem., Int. Ed. Engl.* **1996**, *35*, 1510. Spatz, J. P.; Sheiko, S.; Möller, M. *Macromolecules* **1996**, *29*, 3220.

(17) Bates, F. S.; Fredrickson, G. H. *Annu. Rev. Phys. Chem.* **1990**, *41*, 525.

(18) Matsen, M. W.; Schick, M. *Phys. Rev. Lett.* **1994**, *72* (16), 2660.

(19) Hajduk, D. A.; Harper, P. E.; Gruner, S. M.; Honeker, C. C.; Kim, G.; Thomas, E. L.; Fetters, L. J. *Macromolecules* **1994**, *27*, 4063.

(20) Khandpur, A. K.; Förster, S.; Bates, F. S.; Hamley, I. W.; Ryan, A. J.; Bras, W.; Almdal, K.; Mortensen, K. *Macromolecules* **1995**, *28*, 8796.

(21) Hillmyer, M. A.; Bates, F. S.; Almdal, K.; Mortensen, K.; Ryan, A. J.; Fariclough, J. P. A. *Science* **1996**, *271*, 976.

(22) Matsen, M. W.; Bates, F. S. *Macromolecules* **1996**, *29*, 7641.

(23) Mitchell, D. J.; Tiddy, G. J. T.; Waring, L.; Bostock, T.; McDonald, M. P. *J. Chem. Soc., Faraday Trans. 1* **1983**, *79*, 975.

(24) Yoshikiyo, M. *Micelles: Theoretical and Applied Aspects*; Plenum Press: New York, 1992.

(25) Israelachivili, J. N. *Intermolecular and Surface Forces*, 2nd ed.; Academic Press: London, 1992.

(26) Davis, H. T. *Colloids Surf., A: Physicochemical and Engineering Aspects* **1994**, *91*, 9.

(27) Evans, D. F. *The Colloidal Domain Where Physics, Chemistry, Biology, and Technology Meet*; VCH Publisher: New York, 1994; p 425.

(28) Kaler, E. W.; Murthy, A. K.; Rodriguez, B. E.; Zasadzinski, T. A. *Science* **1989**, *245*, 1371.

(29) Brasher, L. L.; Herrington, K. L.; Kaler, E. W. *Langmuir* **1995**, *11*, 4267.

(30) Engbert, J.; Kevelam, J. *Curr. Opin. Colloid Interface Sci.* **1996**, *1*, 779.

(31) Helm, C. A.; Israelachivili, J. N.; McGuiggan, P. M. *Science* **1989**, *246*, 919.

(32) Safran, S. A.; Pincus, P.; Andelman, D. *Science* **1990**, *248*, 354.

(33) Yuet, P. K.; Blankschtein, D. *Langmuir* **1996**, *12*, 3802.

(34) Bernardes, A. T. *Langmuir* **1996**, *12*, 5763.
(35) Bergström, M.; Eriksson, J. C. *Langmuir* **1998**, *14*, 288.
(36) Laughlin, R. G. *Colloids Surf., A: Physicochemical and Engineering Aspects* **1997**, *128*, 27.
(37) Mortensen, K. *Europhys. Lett.* **1992**, *19* (7), 599. Glatter, O.; Scherf, G.; Schillen, K.; Brown, W. *Macromolecules* **1994**, *27*, 6046.
(38) Wanka, G.; Hoffmann, H.; Ulbricht, W. *Macromolecules* **1994**, *27*, 4145.
(39) Linse, P. *Macromolecules* **1994**, *27*, 4145. Noolandi, J.; Shi, A.-C.; Linse, P. *Macromolecules* **1996**, *29*, 5907.
(40) Chu, B.; Zhou, Z. In *Nonionic Surfactants: Polyoxyalkylene Block Copolymers*; Nace, V. M., Ed.; Marcel Dekker: New York, 1996; pp 67.
(41) Alexandridis, P.; Olsson, U.; Lindman, B. *J. Phys. Chem.* **1996**, *100*, 280. Alexandridis, P.; Olsson, U.; Lindman, B. *Langmuir* **1997**, *13*, 23.
(42) Alexandridis, P.; Holmqvist, P.; Lindman, B. *Colloids Surf., A: Physicochemical and Engineering Aspects* **1997**, *130*, 3.
(43) Alexandridis, P.; Olsson, U.; Lindman, B. *Langmuir* **1998**, *14*, 2627.
(44) Dan, N.; Safran, S. A. *Macromolecules* **1994**, *27*, 5766. Izzo, D.; Marques, C. M. *Macromolecules* **1997**, *30*, 6544.
(45) Hamley, I. W.; Fairclough, J. P. A.; Ryan, A. J.; Ryu, C. Y.; Lodge, T. P.; Gleeson, A. J.; Pedersen, J. S. *Macromolecules* **1998**, *31*, 1188.
(46) Lide, D. R. *CRC Handbook of Chemistry and Physics*, 79th ed.; CRC Press: New York, 1998; pp 3-114, 4-94.
(47) Creutz, S.; Stam, J. V.; Antoun, S.; Schryver, F.; Jérôme, R. *Macromolecules* **1997**, *30*, 4078. Underhill, R.; Ding, J.; Birss, V.; Liu, G. *Macromolecules* **1997**, *30*, 8298.
(48) Tian, M.; Qin, A.; Ramireddy, C.; Webber, S. E.; Munk, P.; Tuzar, Z.; Procházka, K. *Langmuir* **1993**, *9*, 1741.
(49) Zhong, X.-F.; Varshney, S. K.; Eisenberg, A. *Macromolecules* **1992**, *25*, 7160.
(50) Shen, H.; Zhang, L.; Eisenberg, A. *J. Phys. Chem. B* **1997**, *101*, 4697.
(51) Chen, L.; Shen, H.; Eisenberg, A. *J. Phys. Chem. B* **1999**, *103*, 9488.
(52) Baines, F. L.; Armes, S. P.; Billingham, N. C.; Tuzar, Z. *Macromolecules* **1996**, *29*, 8151.
(53) Gao, Z.; Eisenberg, A. *Macromolecules* **1993**, *26*, 7353.
(54) Shen, H.; Eisenberg, A. *Macromolecules*, submitted.
(55) Zhang, L.; Barlow, R. J.; Eisenberg, A. *Macromolecules* **1995**, *28*, 6055.
(56) Menger, F. M.; Gabrielson, K. *J. Am. Chem. Soc.* **1994**, *116*, 1567.
(57) The N_{agg} value given here was obtained for samples equilibrated at 11.5 wt % water, near the sphere/rod-to-rod transition. In the following paper, the N_{agg} value is given for rods at 25.9 wt % water, near the rod/vesicle-to-vesicle transition.
(58) Allen, C.; Yu, Y.; Maysinger, D.; Eisenberg, A. *Bioconjugate Chemistry* **1998**, *9*, 564. Allen, C.; Yu, Y.; Eisenberg, A.; Maysinger, D. *Biochim. Biophys. Acta: Biomembranes*, in press.